


Article

Experimental Study on the Mechanical and Acoustic Emission Characteristics of Tuff with Different Moisture Contents

Wenlong Dong ¹, Lijun Han ^{1,*}, Lingdong Meng ¹, Hexuan Zhu ¹, Shuai Yan ¹, Changyu Xu ¹ and Yanning Dong ²

¹ State Key Laboratory for Geomechanics and Deep Underground Engineering, China University of Mining and Technology, Xuzhou 221116, China

² Anhui Masteel Luohe Mining Co., Ltd., Hefei 231500, China

* Correspondence: hanlj666@163.com

Abstract: Rock materials are often affected by water in underground engineering. In this study, the mechanical and failure characteristics of tuff under different moisture content were studied using laboratory tests. The moisture content variation of tuff was studied in water absorption tests, and the mechanical and failure characteristics of tuff under different moisture contents were studied through uniaxial compression tests with a Micro-II acoustic emission (AE) control acquisition system. The results showed that the moisture content of tuff increases rapidly at the initial stage of water absorption tests and stabilizes after 180 h of immersion. According to the results of uniaxial compression tests, both uniaxial compressive strength and elasticity modulus decreased with the increase in moisture content. The AE parameters analyses showed that, when the moisture content increased, the accumulated AE counts and energy gradually decreased, and the “quiet period” at the initial stage of uniaxial compression tests lasted longer, and the RA (rise time/amplitude)–AF (AE counts/duration) distribution and the failure characteristics verified that the failure patterns evolved from shear failure to tensile failure. Scanning electron microscopy was used to observe the morphology of the fracture surface and analyze the influence of moisture content on the fracture characteristics of the tuff at the mesoscopic level. The results of this research can be used as a basis for studying the influence of water on tuff.

Keywords: moisture content; uniaxial compression test; rock acoustic emission; SEM; rock failure mode



Citation: Dong, W.; Han, L.; Meng, L.; Zhu, H.; Yan, S.; Xu, C.; Dong, Y. Experimental Study on the Mechanical and Acoustic Emission Characteristics of Tuff with Different Moisture Contents. *Minerals* **2022**, *12*, 1050. <https://doi.org/10.3390/min12081050>

Academic Editors: Abbas Taheri and Alison Ord

Received: 22 June 2022

Accepted: 18 August 2022

Published: 20 August 2022

Publisher's Note: MDPI stays neutral with regard to jurisdictional claims in published maps and institutional affiliations.



Copyright: © 2022 by the authors. Licensee MDPI, Basel, Switzerland. This article is an open access article distributed under the terms and conditions of the Creative Commons Attribution (CC BY) license (<https://creativecommons.org/licenses/by/4.0/>).

1. Introduction

As underground projects such as tunnels, mining, and underground chambers are built in deeper and more complex geological environments, surrounding rocks will be more significantly affected by groundwater. The presence of groundwater increases the moisture content of rocks, and a large number of experiments and studies have shown that the increase in moisture content leads to a decrease in the strength and deformation properties of rocks, which will cause many rock engineering disasters [1–3]. Under the influence of groundwater, the engineering properties of the surrounding rock will be degraded to a certain extent, which will greatly affect the stability and safety of the projects [4]. Therefore, it is quite essential for the safety evaluation of underground engineering to carry out in-depth research on the deterioration of rock properties and failure characteristics under different moisture content.

Tuff is a common volcanic clastic rock, formed by the transport, scattering, cementation, and deposition of volcanic ash from volcanic eruptions, and it is widely distributed in southeastern China. Tuff is a widely existing rock in underground engineering, which often endangers the stability and safety of engineering under the influence of water. Therefore, it is of great meaning to study the influence of moisture content on the properties of tuff.

In recent years, acoustic emission (AE) technology has been widely used in geotechnical engineering monitoring as a nondestructive testing technology [5]. The AE phenomenon

refers to the elastic wave phenomenon generated by the rapid release of the local stress energy that propagates through the material. The AE signals collected by the AE collection device contain a large amount of information about the material cracks, and the amplitude, frequency, count, and energy obtained are widely used in the material failure process and failure characteristic analysis [6–9]. As a kind of brittle material, a large number of microcracks and fracture extensions will be generated inside the specimens during the process from initial loading to damage, and several AE events will be generated along with this process. By analyzing the AE characteristics parameters of rocks during the damage process, the failure characteristics of rocks under different moisture content can be effectively analyzed.

Previously, many scholars conducted numerous studies on the failure characteristics of rocks under different moisture content. Yao et al. [10] conducted uniaxial compression tests on coal, mudstone, and siltstone under different water absorption times, and they found that the uniaxial compressive strength, elastic modulus, and peak strain of coal and rock specimens all decreased to a certain extent as the moisture content increasing. Zhou et al. [11] analyzed the water influence on the mechanical behavior of rock in saturation and drying processes under static and dynamic tests. Vasarhelyi [12] studied the variations of porosity, uniaxial compressive strength, elastic modulus, and tensile strength of limestone at different water content. Yilmaz [13] studied the degradation of gypsum rock mechanical property parameters by uniaxial compression test under moisture content and obtained the law that the uniaxial compressive strength and elastic modulus of gypsum rock decreased with the growth of water content. Vishal et al. [14] studied the strength characteristics of saturated coal and rock mass and the initiation of internal micro-cracks under high-stress conditions. Yu et al. [15] studied the influence of moisture content on the mechanical properties and crack propagation of siltstone through uniaxial compression tests, and they proved that the moisture content was negatively linearly correlated with peak stress and elastic modulus. Roy et al. [16] conducted experimental research on the fracture and mechanical properties of saturated sedimentary rocks, and the results showed that saturability had a significant effect on the peak stress and fracture properties of sedimentary rocks. In addition, the Brazilian split strength and fracture toughness decreased with the increase in saturation.

AE technology can monitor the initiation and development of microcracks in the failure process of rock specimens, thereby revealing the evolution of internal damage and failure of the rock. In view of the advantage, AE technology has been used to conduct several studies on rock failure mechanism [17–23]. Liu et al. [8] studied the influence of strain rate on AE characteristic parameters and rock failure characteristics through experiments, and they obtained the law that the cumulative AE counts decreased as a power function with increasing strain rate. Chen et al. [24] used AE technology to study the law of fracture development during the hydraulic fracturing tests process, thereby revealing the fracture mechanism of fluid–solid interaction during hydraulic fracturing. Chen et al. [25] conducted uniaxial compression tests and AE monitoring on siltstones under different water saturation levels, and they studied the relationship between AE characteristic parameters and siltstone crack propagation with different moisture content. The results of the tests showed that the AE count rate decreased gradually during the compaction process as the moisture content of siltstone increased. Carpinteri et al. [26] conducted uniaxial compression tests with AE monitoring on concrete and rock specimens, revealing the law of energy absorption and release during the compression process of brittle materials. According to the study of AE parameters, it was proven that the heterogeneity of various properties of partly soaked coal specimens was more distinct than that of completely soaked and non-soaked coal specimens. Amann et al. [27] studied the brittle failure characteristics of clay using uniaxial compression tests and AE technology. The test results showed that the crack initiation threshold was about 30% of the peak stress, and the crack damage threshold was about 70% of the peak stress. Xiao et al. [28] used AE and infrared characterization methods to monitor coal samples with different moisture content

under uniaxial compression tests, revealing the overall and surface damage variables and their evolution. The test results showed that the internal damage of the coal specimens preceded the external damage, and the appearance of the AE signal was earlier than the abnormal infrared point. Rodriguez and Celestino [29] conducted splitting tests and AE monitoring on marble and granite, and the results showed that the internal cracks development processes and cracking types of the rock were mainly determined by the rock mineral composition.

In this article, tuff specimens with different moisture content were prepared and used to study the variation of mechanical and acoustic emission characteristics of tuff with moisture content through a uniaxial compression test and acoustic emission monitoring system. Then, scanning electron microscopy (SEM) was used to study the mesoscopic characteristics of tuff under different moisture content and verified the macroscopic failure characteristics at the micro level.

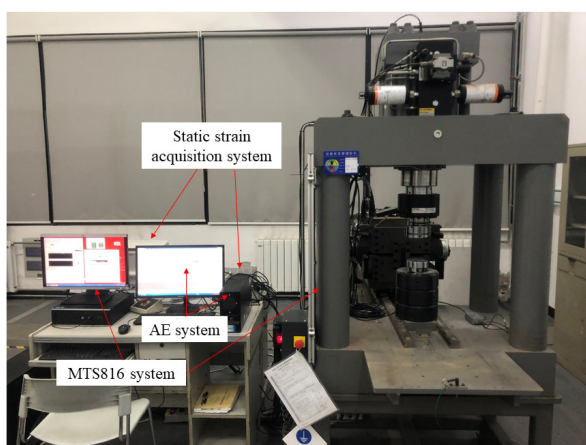
2. Materials and Methods

2.1. Specimen Preparation

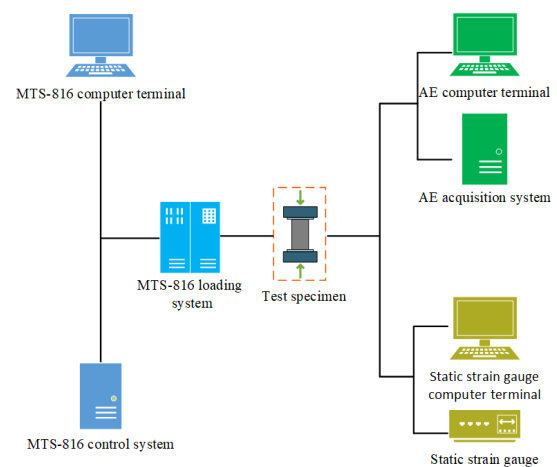
The tuff specimens used in this study were taken from the Luohe Iron Mine located in Hefei, Anhui Province, China. In order to satisfy the requirements of uniaxial compression tests, the rock specimens were made into a cylinder of $\phi 50 \text{ mm} \times H100 \text{ mm}$ in accordance with the recommended standards of the International Society for Rock Mechanics (ISRM). Both ends of all specimens were ground to obtain a flat surface. There were 27 specimens in total, which required drying before testing. All specimens were placed in the oven and dried at $110 \text{ }^\circ\text{C}$ for 24 h, before being placed into a desiccator and weighed. The specimens were divided into nine groups of three specimens each and subjected to water absorption tests through free absorption. In order to obtain specimens with different moisture contents, the immersion time was set to 0 h, 6 h, 12 h, 24 h, 60 h, 180 h, 450 h, and 960 h, and the last group of specimens was forcibly saturated.

2.2. Experimental Equipment and Procedure

An MTS-816 electrohydraulic servomechanical test system was employed to carry out the uniaxial compression tests, with the loading rate set to 0.1 mm/min . Vaseline was applied to both ends of the specimens to eliminate the influence of end face constraints. A Micro-II AE acquisition system was used to monitor AE signals (seen in Figure 1), and the AE parameters were acquired by the AE sensor affixed on the surface of the specimens. A DH3816N static strain collection system was used to acquire strain data, as shown in Figure 2.



(a)



(b)

Figure 1. Testing system: (a) diagram of testing system; (b) layout of testing system.

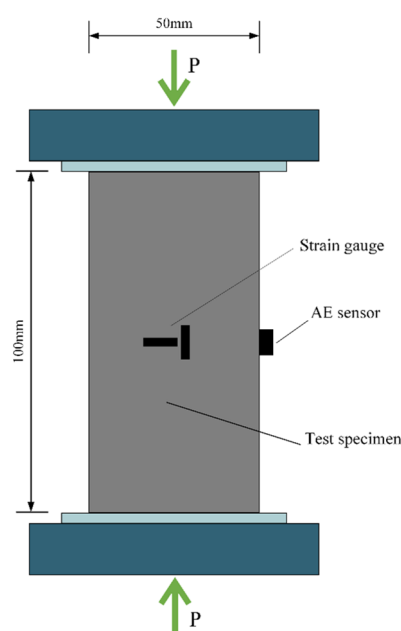


Figure 2. Sensor layout on the surface of specimen.

The acquisition parameters of the AE system for this study were set as shown in Table 1.

Table 1. Acquisition parameters of the AE system.

Parameter	MSPS	Threshold (dB)	HLT (μ s)	HDT (μ s)	PDT (μ s)	Resonant Frequency (kHz)	Pre-Amplified (dB)
Value	1	40	1000	800	200	300	40

MSPS is the sampling rate; HLT, HDT, and PDT denote the hit lockout time, hit definition time, and peak definition time, respectively.

3. Experimental Results and Discussion

3.1. Relationship between Moisture Content and Immersion Time

The specimens were subjected to water absorption tests, and the moisture contents varied with the time of immersion. The saturated specimens were prepared by boiling the specimens for 6 h after immersion. The moisture content and average moisture content data of the specimens are shown in Table 2.

The relative relationship between average moisture content and immersion time is shown in Figure 3. With the increase in immersion time, the average moisture content showed an upward trend. During the immersion time from 0 h to 24 h, the moisture content increased rapidly, which was mainly due to the rapid water absorption on the surface of the specimens at the initial stage of immersion. From 24 h to 180 h, the moisture content still showed an upward trend with the accumulation of immersion time, but the rising rate dropped rapidly. This was mainly due to the slower rate of water infiltration into the interior of rock after the surfaces of the specimens were soaked by water. From 180 h to 960 h, the moisture content of the tuff specimens continued to increase with immersion time, but the rising rate was very small, and the moisture content was close to the saturation state in value. This was mainly because the pores that allow water to penetrate freely were basically occupied by water; thus, the water absorption rate of the rock became very slow. Accordingly, it was difficult for water to penetrate into the rock specimens during this stage. After being immersed in water for 960 h, the average moisture content of the specimens was 1.02%, and the average saturated moisture content was 1.05%, which were very close to each other.

Table 2. Results of water absorption test.

No.	Immersion Time	Dry Weight (g)	Wet Weight (g)	Moisture Content (%)	Average Moisture Content (%)
A-1	0 h	667.28		0	0
A-2		658.17		0	
A-3		649.84		0	
B-1	6 h	669.93	671.87	0.30	0.28
B-2		662.31	664.10	0.27	
B-3		652.79	654.55	0.26	
C-1	12 h	663.80	666.39	0.39	0.40
C-2		671.15	673.90	0.41	
C-3		661.26	663.91	0.4	
D-1	24 h	646.68	650.69	0.62	0.60
D-2		647.25	651.07	0.59	
D-3		658.74	662.69	0.6	
E-1	60 h	660.41	665.63	0.79	0.81
E-2		656.28	661.60	0.81	
E-3		644.91	650.20	0.82	
F-1	180 h	655.21	661.04	0.88	0.90
F-2		647.26	653.02	0.90	
F-3		655.95	661.92	0.91	
G-1	450 h	649.58	655.82	0.96	0.97
G-2		644.32	650.63	0.99	
G-3		656.28	662.71	0.97	
H-1	960 h	651.79	658.37	1.01	1.02
H-2		647.66	654.27	1.02	
H-3		649.57	656.33	1.04	
I-1	Saturated	649.39	656.21	1.05	1.05
I-2		654.92	661.73	1.04	
I-3		651.74	658.71	1.07	

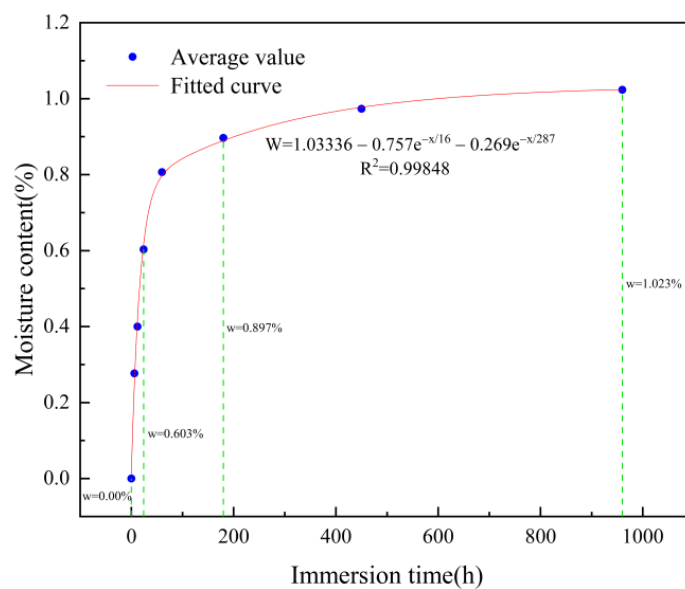


Figure 3. Relationship between moisture content and immersion time.

The relationship between the average moisture content and the immersion time obtained in the tests revealed the relationship of the sample moisture content with the immersion time, which could be fitted using Equation (1).

$$\omega = 1.03336 - 0.757e^{-x/16} - 0.269e^{-x/287}, \tag{1}$$

where ω denotes the average moisture content, and x represents the specimen immersion time. The correlation coefficient of the fitted function was $R^2 = 0.99848$, proving that the formula could accurately characterized the relationship.

3.2. Mechanical Behavior of Tuff under Different Moisture Content

The results of the uniaxial compression tests are listed in Table 3. As shown in Figure 4, the peak stress gradually declined with the increase in moisture content. The stress–strain curves of all specimens showed a concave upward trend in the initial loading stage, which was mainly due to the nonlinear deformation caused by the crack closure in the rock specimens. With the increase in load, the stress–strain curves showed an approximately linear growth, with a lower moisture content resulting in a higher growth rate. With continued loading, the stress–strain curve reached the peak stress after going through a downward concave section. In addition, both the peak stress and the corresponding strain gradually decreased as the moisture content increased.

Table 3. Results of uniaxial compression tests.

No.	Immersion Time	UCS (MPa)	Average UCS (MPa)	Elasticity Modulus (GPa)	Average Elasticity Modulus (GPa)	Poisson's Ratio	Average Poisson's Ratio
A-1	0 h	170.01	170.05	18.06	17.95	0.20	0.19
A-2		170.53		17.96		0.18	
A-3		169.61		17.82		0.19	
B-1	6 h	158.09	157.59	17.07	16.97	0.21	0.23
B-2		157.57		16.93		0.24	
B-3		157.11		16.90		0.23	
C-1	12 h	144.85	146.39	16.26	16.41	0.23	0.25
C-2		148.10		16.56		0.26	
C-3		146.22		16.41		0.27	
D-1	24 h	128.96	127.84	16.30	16.05	0.27	0.27
D-2		127.36		16.11		0.26	
D-3		127.20		15.73		0.27	
E-1	60 h	120.78	119.83	15.81	15.69	0.27	0.27
E-2		119.89		15.66		0.29	
E-3		118.82		15.60		0.26	
F-1	180 h	112.26	112.16	15.42	15.39	0.28	0.28
F-2		111.35		15.48		0.30	
F-3		112.88		15.26		0.26	
G-1	450 h	108.22	107.27	15.00	15.19	0.27	0.29
G-2		107.73		15.22		0.30	
G-3		105.87		15.34		0.30	
H-1	960 h	105.41	104.88	15.12	15.09	0.30	0.30
H-2		105.16		14.94		0.29	
H-3		104.07		15.20		0.31	
I-1	Saturated	103.14	103.03	15.01	15.01	0.29	0.30
I-2		103.02		14.99		0.31	
I-3		102.93		15.02		0.31	

The UCS refers to the uniaxial compressive strength.

In addition, the stress–strain curve presented different development trends under different moisture contents after peak stress. For the dry specimens, the peak stress obtained by the tests reached the maximum value, and the stress–strain curve had no obvious post-peak segment, indicating a brittle failure mode. The peak stress gradually decreased with the increase in moisture content, and the post-peak segments gradually emerged. Furthermore, a greater moisture content led to a more obvious post-peak segment. It can be seen from the results that, when the moisture content increased, the tuff specimen showed a certain bearing capacity after failure, which presented an obvious enhancement of plasticity and toughness.

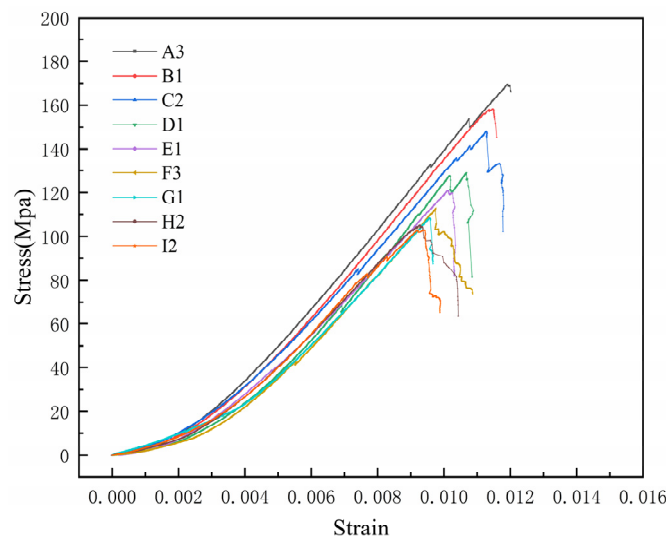


Figure 4. Stress–strain curve of specimens with different moisture content.

The variation law of peak stress and average UCS with moisture content is shown in Figure 5. The peak stress of the specimens showed a downward trend as the moisture content increased, but the decline rate was not maintained at a constant value. The peak stress decline rate was maintained at a relatively high level during the initial stage of increasing moisture content. However, as the moisture content continued to increase, the decline rate of the peak stress gradually dropped. The results indicate that the weakening effect of water on the strength of the tuff gradually decreased after the moisture content reached a certain level. The relative relationship between peak stress and moisture content could be fitted using Equation (2).

$$y = 17.128 + 158.365e^{-0.564x}, \tag{2}$$

where y is the uniaxial compressive strength, and x denotes the moisture content. The correlation coefficient of the fitted function was $R^2 = 0.98242$.

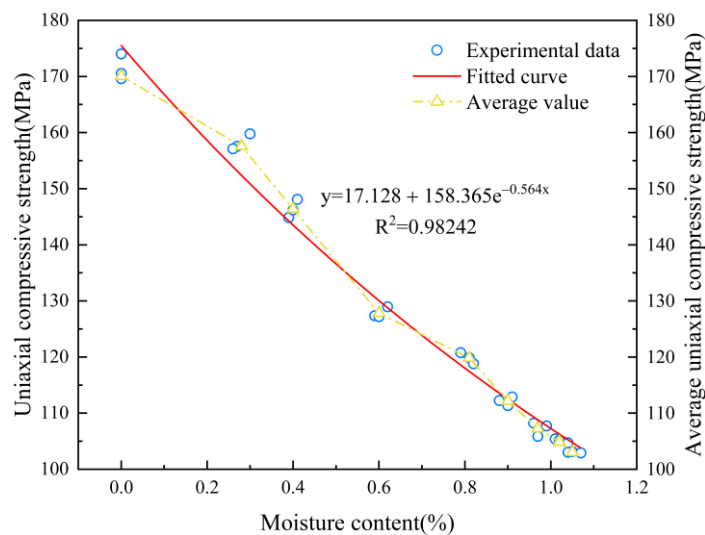


Figure 5. Relationship between uniaxial compressive strength and moisture content.

As shown in Figure 6, the average elastic modulus showed a downward trend as the moisture content increased, but the decline rate of the elastic modulus gradually dropped. When the specimens were dry, the average value of elastic modulus was 17.95 GPa, whereas, when the specimen was saturated, the average value of elastic modulus decreased to

15.01 GPa, with a decrease of 16.38%. This demonstrated that water produced an obvious decrease in the elastic modulus of the tuff. The relationship between the average value of the elastic modulus and the moisture content could be fitted using Equation (3).

$$y = 12.766 + 5.161e^{-0.767x}, \quad (3)$$

where y is the elastic modulus, and x denotes the moisture content. The correlation coefficient of the fitted function was $R^2 = 0.99331$.

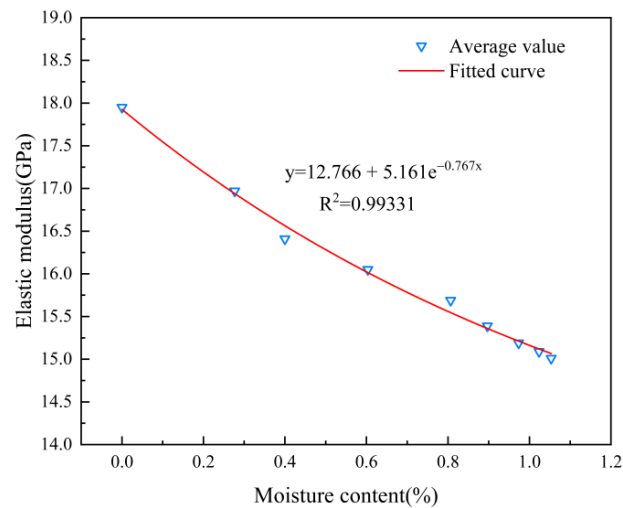


Figure 6. Relationship between elastic modulus and moisture content.

The Poisson's ratio of the tuff specimens gradually increased with the increase in moisture content (Figure 7). The average Poisson's ratio of the dry specimens was 0.19, whereas the average Poisson's ratio of the saturated specimens was 0.30, showing an increase of 57.89%. The results proved that the increase in moisture content caused a large increase in the Poisson's ratio of the tuff specimens. In addition, the Poisson's ratio was more affected by moisture content than the elastic modulus. The relationship between the average Poisson's ratio and the moisture content could be fitted using Equation (4).

$$y = 0.342 - 0.152e^{-1.126x}, \quad (4)$$

where y represents Poisson's ratio, and x denotes the moisture content. The correlation coefficient of the fitted function is $R^2 = 0.97451$.

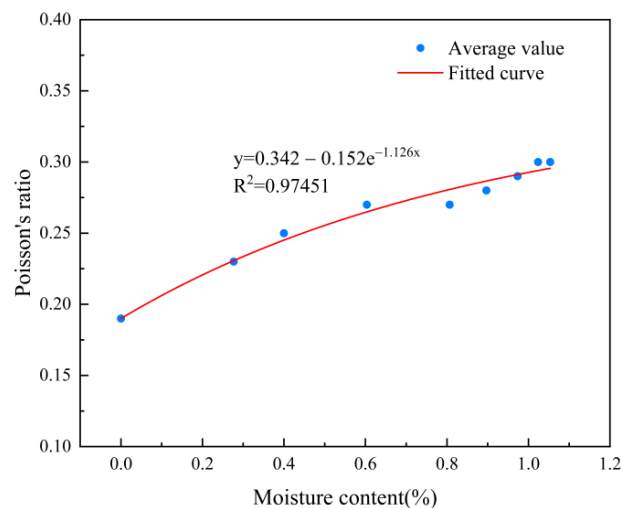


Figure 7. Relationship between Poisson's ratio and moisture content.

Many scholars have studied the influence of moisture content on the mechanical characteristics of other types of rocks, such as sandstone, red sandstone, marble, and siltstone, and found that the weakening effect of water will make the mechanical parameters such as uniaxial compressive strength and elastic modulus show similar change trends [25,30–32].

3.3. AE Counts and Energy Characteristics of Tuff with Different Moisture Content

The stress and AE parameter results with time under different moisture content in uniaxial compression tests are demonstrated in Figure 8, representing the nine different moisture states. The AE parameters collected during the tests included AE counts, amplitude, and energy, which showed a good correlation with stress evolution as a function of loading. During the uniaxial compression tests, the stress of the specimens was low at the initial loading stage, and the AE signals were rarely collected. With the increase in stress, the AE energy and accumulated counts increased gradually and showed a significant growth when the specimens were about to fail. This proved that the AE energy and accumulated counts had a good correlation with the crack propagation and failure of the specimens during loading.

During the initial loading period of uniaxial compression tests, there was a “quiet period” with few cracks being generated and expanding within the rock. AE events hardly occurred at this stage. When the moisture content of the specimens was 0, as shown in Figure 8a, the AE counts started to accumulate at about 151 s, and the AE events occurred earlier compared with the other specimens. As the moisture content increased, the AE events occurred later. When the specimens were saturated, as shown in Figure 8i, the AE counts started to accumulate at 246 s. The test results showed that the duration of the “quiet period” increased significantly with the moisture content during the uniaxial compression tests, which further confirmed that the initiation time of cracks within the tuff became later and later with the increase in moisture content.

The AE signals began to accumulate after the “quiet period”. The AE counts basically rose steadily according to a certain slope before the peak stress, and the AE energy was also collected with the generation of AE events. However, both the growth rate of accumulated AE counts and the AE energy value were kept at a low level. When the stress reached the peak value, the accumulated AE counts and energy showed a very significant increase, which indicated that a large number of fracture events with high energy release occurred in the specimens when destroyed.

The information of AE parameters during the tests of the specimens with different moisture content showed different characteristics. With the increase in moisture content, the accumulated AE counts and energy value both presented a gradually decreasing trend. When the moisture content was low, the AE energy appeared more frequently with a higher value. However, as the moisture content increased, the occurrence of AE events became sparse, and the value of AE energy was relatively reduced, as shown in Figure 8. The analysis of AE parameters also revealed that a higher moisture content resulted in a lower AE energy and fewer accumulated AE counts at the peak stress. Compared with dry specimens, the accumulated AE counts of saturated specimens decreased by an order of magnitude, and the maximum AE energy also decreased by 32.86%. This was mainly due to the softening effect on the tuff specimens caused by water. Higher moisture content of the specimens led to less internal fracture generation, expansion, and penetration during the loading process, and less energy was released at the same time. Although the overall energy value showed a downward trend when the moisture content increased, this did not affect the phenomenon of sudden energy bursts when the specimens were destroyed.

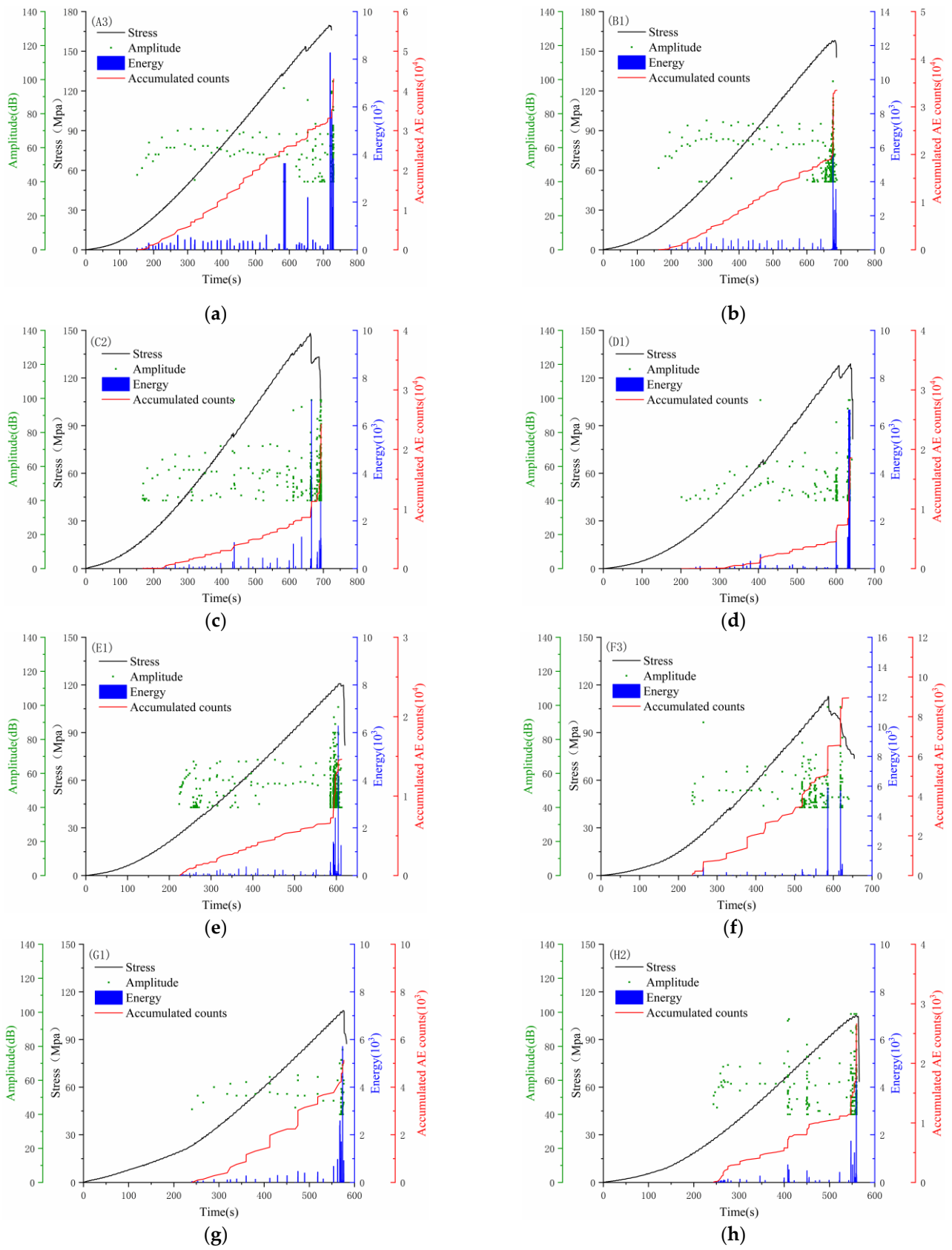


Figure 8. Cont.

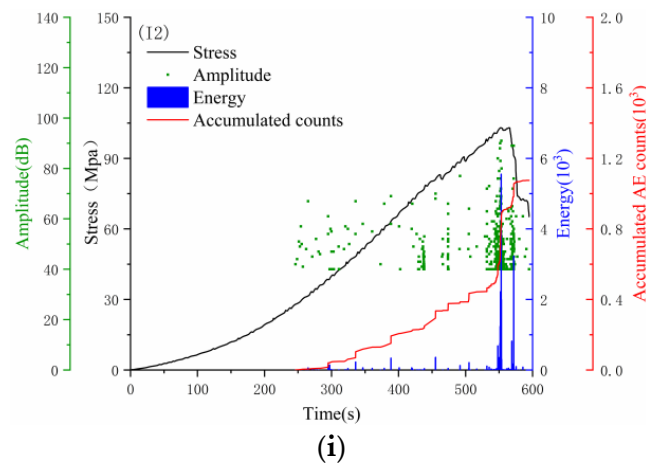


Figure 8. The evolution of stress, AE energy, accumulated AE counts, and amplitude with time under different moisture content. (a–i) Specimens under different moisture content.

3.4. RA–AF Distribution and Tuff Failure Characteristics under Different Moisture Content

The ratio of the rise time to the amplitude of an AE event was recorded as the RA value, and the ratio of the AE counts to the duration time was recorded as the AF value. The RA value and AF value are very important AE parameters to analyze the rock failure process. The combined analysis of RA and AF is often used to determine the fracture type in the analysis of rock fracture generation mechanisms [33–35]. Their definitions are shown in Equations (5) and (6).

$$RA = \text{Rise time} / \text{Amplitude.} \tag{5}$$

$$AF = \text{AE counts} / \text{Duration.} \tag{6}$$

The RA–AF distribution analysis was implemented in a rectangular coordinate system with RA value as the horizontal axis and AF value as the vertical axis. During the uniaxial compression tests, a lower RA value and a higher AF value are generated when tensile cracks occurred. In contrast, the generation of shear cracks results in a higher RA value and a lower AF value. A diagonal line was used to divide the rectangular coordinate system into a tensile crack region and a shear crack region, as shown in Figure 9.

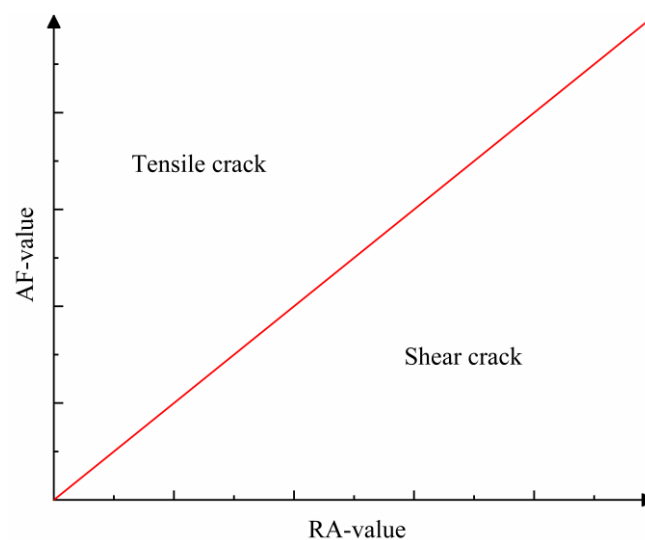


Figure 9. Relationship between crack types and RA–AF distribution.

The RA value and AF value were normalized and then drawn in the coordinate system, as shown in Figure 10. It can be seen from the RA–AF distribution that the RA–AF values

were mainly distributed along the horizontal axis when the moisture content was 0. The RA values were higher, and the AF values were lower, being mainly distributed in the shear crack region, as shown in Figure 10a. This phenomenon revealed that the cracks generated within the rock were mainly shear cracks when the rock specimens were dry. When the moisture content increased, the distribution of RA–AF values gradually transited from the shear crack region to the tension crack region. As shown in Figure 10c, when the moisture content reached 0.41%, RA–AF values were evenly distributed in the tensile and shear crack region. Therefore, both shear cracks and tension cracks were generated under this moisture content, and these two types of cracks were relatively close in number. For saturated specimens, the RA–AF values were mainly distributed along the longitudinal axis. The RA values were lower, and the AF values were higher, being mainly distributed in the tensile crack region, as shown in Figure 10i. This means that the majority of cracks generated inside the specimens were tension cracks when saturated.

The variation of RA–AF distribution was very significant at the initial stage of the rising process of moisture content. When the moisture content was higher than 0.6%, as shown in Figure 10e–i, the RA–AF distribution tended to be stable and mainly concentrated in the tensile crack region. The results showed that the cracks generated during the uniaxial compression tests were mainly tensile cracks when the moisture content of the specimens reached a certain level, and the crack type no longer changed with the continued increase in moisture content.

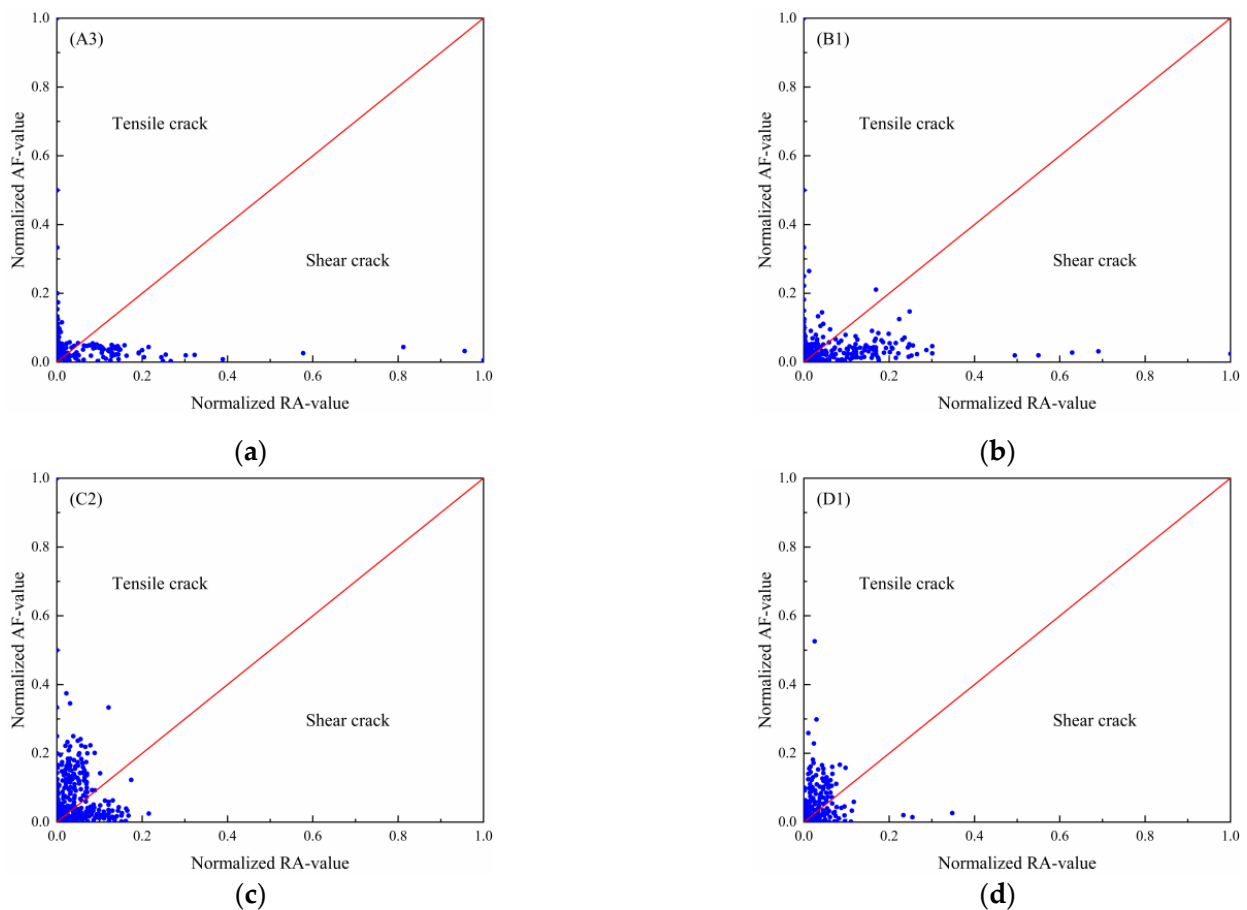


Figure 10. Cont.

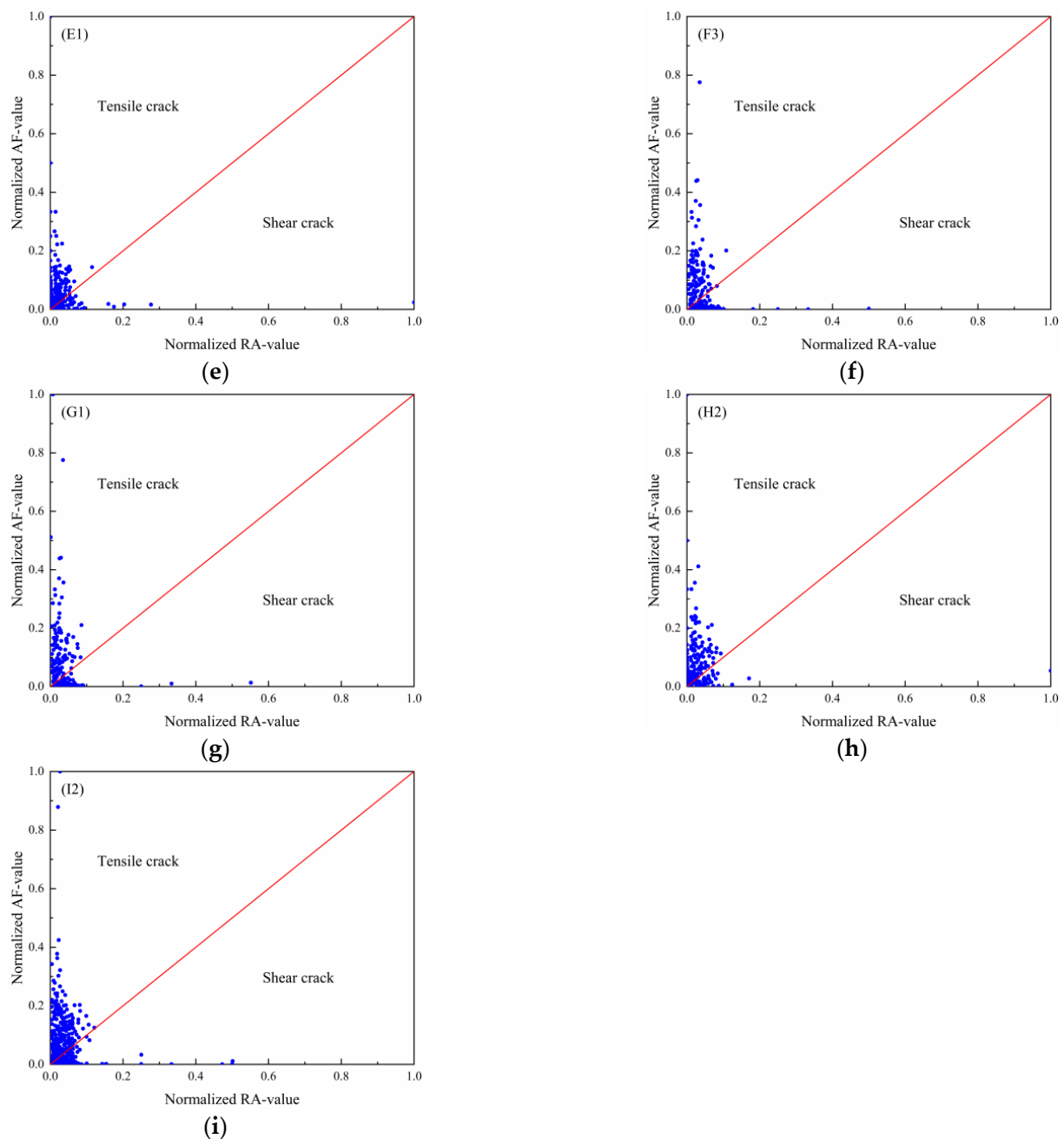


Figure 10. RA–AF distribution of tuff specimens with different moisture content. (a–i) Specimens under different moisture content.

The failure patterns of the tuff specimens after the tests are shown in Figure 11. The failure characteristics demonstrated that the crack types were mainly diagonal shear cracks when the moisture content of the specimens was low. The failure pattern was mainly manifested as shear slip along the oblique cracks, as shown in Figure 11a–c. During the process of increasing moisture content, the type of cracks gradually changed from shear cracks along the diagonal to tensile cracks along the longitudinal. As shown in Figure 11h,i, the cracks produced were mainly tensile cracks when the specimens failed under high moisture content, and the failure pattern was mainly manifested as splitting tensile failure. In addition, through the comparison of the test results, it was found that the tuff specimens had a higher level of fragmentation under high moisture content, and more fragments were produced when they were broken.

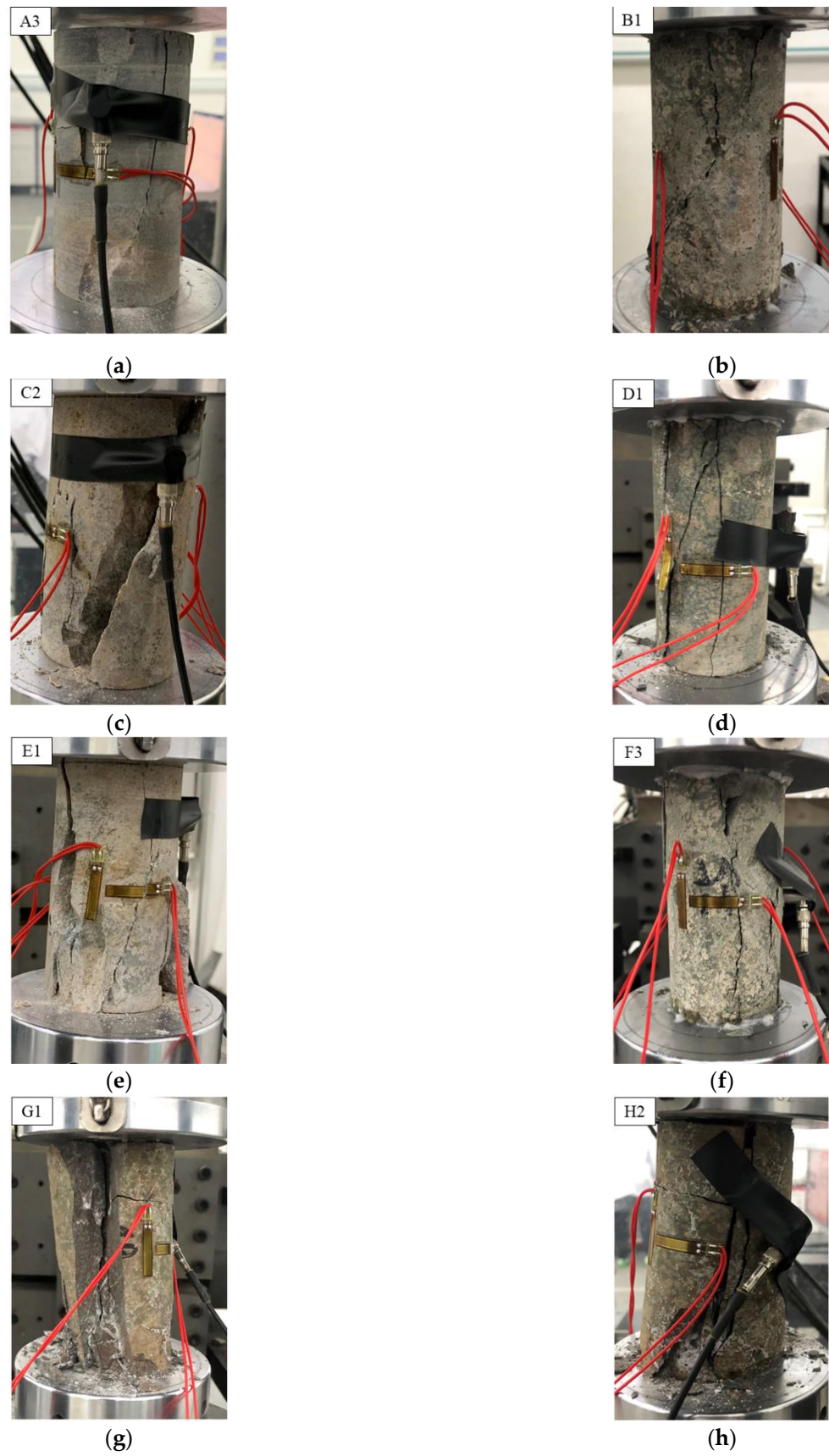


Figure 11. Cont.



Figure 11. Failure patterns of tuff specimens under different moisture content. (a–i) Specimens under different moisture content.

These experimental phenomena showed that the level of moisture content affected the failure patterns of the tuff specimens. As the moisture content increased, the tuff specimens gradually transitioned from shear failure to tensile failure, and the level of fragmentation gradually increased. This was mainly because of the increased infiltration of water into the rock with the increase in moisture content. Furthermore, the cementation between the mineral particles inside the specimens was weakened, which in turn caused a change in failure pattern and more severe damage when the rock specimens failed.

The fracture characteristics of the tuff specimens in the uniaxial compression tests under different moisture content were basically consistent with the fracture types obtained via the analysis of RA–AF distribution. This further proved that the RA–AF distribution could successfully determine the failure types of tuff specimens under different moisture content in the uniaxial compression test.

3.5. Mesoscopic Analysis of Failure Fracture under Different Moisture Content

In order to study the mesoscopic characteristics of tuff under different moisture content, scanning electron microscopy (SEM) was used to analyze the fracture mesoscopic morphology of the samples.

The damaged samples with 0% (A3), 0.62% (D1), and 1.04% (I2) moisture content were selected for SEM detection of the fracture surface, and the magnification was 2000×. As shown in Figure 12a–c, when the sample was dry, the failure section was relatively neat, and there were fewer fractures of holes and step zones. With the increase in moisture content, the failure mode tended to be complex, and the failure degree was higher, with more holes and cracks appearing. In addition, a higher moisture content led to more step zone cracks.

This is mainly because, with the increase in moisture content, water weakens the cementation of rock, resulting in a higher failure degree of tuff, and more holes and crack zones appear at the fracture surface at the mesoscopic level. This also explains the more serious macroscopic damage of tuff in the case of high moisture content at the microscopic level.

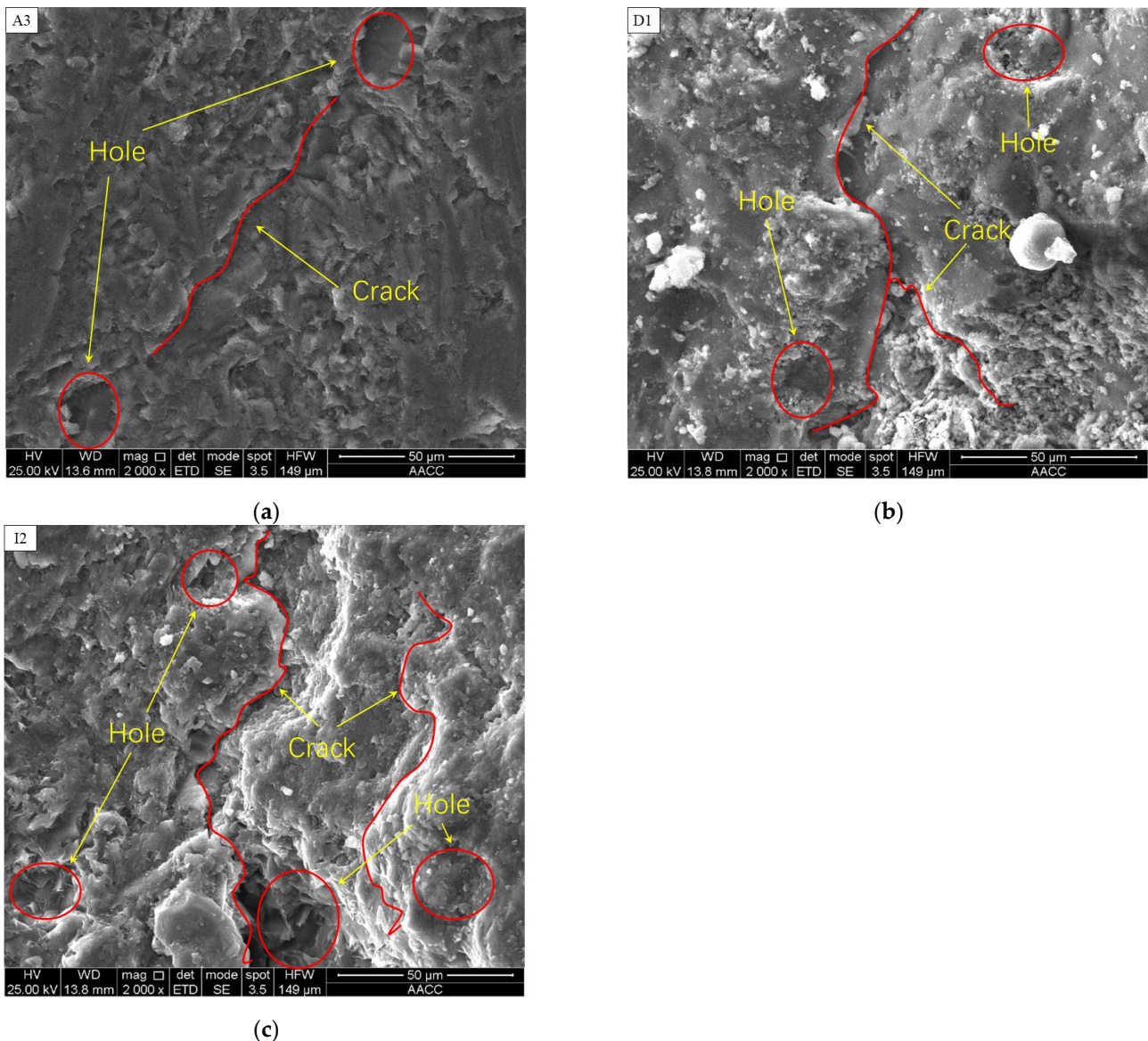


Figure 12. Mesoscopic fracture morphology of the samples under different moisture content according to SEM (2000×): (a) dry specimen; (b) specimen with 0.62% moisture content; (c) saturated specimen.

4. Conclusions

In this article, water absorption tests and uniaxial compression tests were carried out on tuff specimens to study the influence of moisture content on their mechanical and failure characteristics. The AE parameters obtained by the AE monitoring system were applied to analyze the characteristics of crack propagation and failure types in the rock under different moisture contents. The key findings obtained from this study are as follows:

- (1) The moisture content increased with immersion time. At the initial stage of immersion, the moisture content rose rapidly (0–24 h). After 24 h of immersion, the increasing rate of moisture content dropped significantly. After 180 h of immersion, the moisture content gradually stabilized and approached saturation in numerical terms.
- (2) The uniaxial compressive strength and elastic modulus of the tuff specimens both decreased with the increase in moisture content, reaching the lowest values when the specimens were saturated. The uniaxial compressive strength decreased rapidly at the initial stage of immersion, and the decrease rate slowed down as the moisture content increased. The variation of elastic modulus also showed a similar trend. When the moisture content increased, the stress–strain curves showed obvious post-peak

segments, which proved that the increase in moisture content led to an improvement in plasticity and toughness of the tuff. In addition, the Poisson's ratio increased with moisture content.

- (3) Higher moisture content of the tuff specimens led to a longer “quiet period” experienced during the initial loading stage. In addition, the increase in moisture content also led to a decrease in the accumulated AE counts and energy. This proved that the generation and expansion of tuff rock cracks were delayed by the softening effect of water, and the number of internal crack events in the rock was relatively decreased. Furthermore, the energy release generated by internal crack events of the tuff was also reduced.
- (4) When the moisture content of the rock was low (lower than 0.41%), the RA–AF values were mainly distributed along the horizontal axis, indicating that the crack type was dominated by shear crack, whereas, when the rock moisture content was high (higher than 0.41%), the RA–AF values became distributed along the vertical axis, indicating that the crack type was mainly tension crack. The failure morphology of the tuff specimens also further verified that the dominant crack type changed from shear crack to tensile crack with the increase in moisture content, while the disruption at the microscopic level was also more intense.

Author Contributions: Writing—original draft preparation, W.D.; writing—review and editing, L.H. and W.D.; methodology, L.M.; visualization, H.Z. and S.Y.; project administration, C.X.; funding acquisition, L.H. and Y.D.; supervision, L.H. All authors read and agreed to the published version of the manuscript.

Funding: This research was funded by National Natural Science Foundation of China (No. 51574223).

Data Availability Statement: Not applicable.

Acknowledgments: The authors thank Anhui Masteel Luohe Mining Co., Ltd. for the test samples. The authors also sincerely thank the State Key Laboratory for Geomechanics and Deep Underground Engineering, China University of Mining and Technology for providing the test equipment.

Conflicts of Interest: The authors declare no conflict of interest.

References

1. Kim, E.; Changani, H. Effect of water saturation and loading rate on the mechanical properties of Red and Buff Sandstones. *Int. J. Rock Mech. Min. Sci.* **2016**, *88*, 23–28. [[CrossRef](#)]
2. Vasarhelyi, B.; Van, P. Influence of water content on the strength of rock. *Eng. Geol.* **2006**, *84*, 70–74. [[CrossRef](#)]
3. Li, L.P.; Sun, S.Q.; Wang, J.; Yang, W.M.; Song, S.G.; Fang, Z.D. Experimental study of the precursor information of the water inrush in shield tunnels due to the proximity of a water-filled cave. *Int. J. Rock Mech. Min. Sci.* **2020**, *130*, 104320. [[CrossRef](#)]
4. Zhu, J.; Deng, J.H.; Chen, F.; Huang, Y.M.; Yu, Z.Q. Water Saturation Effects on Mechanical and Fracture Behavior of Marble. *Int. J. Geomech.* **2020**, *20*, 04020191. [[CrossRef](#)]
5. Ranjith, P.G.; Jasinge, D.; Song, J.Y.; Choi, S.K. A study of the effect of displacement rate and moisture content on the mechanical properties of concrete: Use of acoustic emission. *Mech. Mater.* **2008**, *40*, 453–469. [[CrossRef](#)]
6. Liu, X.X.; Wu, L.X.; Zhang, Y.B.; Liang, Z.Z.; Yao, X.L.; Liang, P. Frequency properties of acoustic emissions from the dry and saturated rock. *Environ. Earth Sci.* **2019**, *78*, 67. [[CrossRef](#)]
7. Shiotani, T.; Ohtsu, M.; Ikeda, K. Detection and evaluation of AE waves due to rock deformation. *Constr. Build. Mater.* **2001**, *15*, 235–246. [[CrossRef](#)]
8. Liu, X.; Liu, Z.; Li, X.; Gong, F.; Du, K. Experimental study on the effect of strain rate on rock acoustic emission characteristics. *Int. J. Rock Mech. Min. Sci.* **2020**, *133*, 104420. [[CrossRef](#)]
9. Lockner, D. The role of acoustic emission in the study of rock fracture. *Int. J. Rock Mech. Min. Sci. Geomech. Abstr.* **1993**, *30*, 883–899. [[CrossRef](#)]
10. Yao, Q.; Wang, W.; Zhu, L.; Xia, Z.; Tang, C.; Wang, X. Effects of moisture conditions on mechanical properties and AE and IR characteristics in coal–rock combinations. *Arab. J. Geosci.* **2020**, *13*, 615. [[CrossRef](#)]
11. Zhou, Z.L.; Cai, X.; Cao, W.Z.; Li, X.B.; Xiong, C. Influence of Water Content on Mechanical Properties of Rock in Both Saturation and Drying Processes. *Rock Mech. Rock Eng.* **2016**, *49*, 3009–3025. [[CrossRef](#)]
12. Vasarhelyi, B. Statistical analysis of the influence of water content on the strength of the miocene limestone. *Rock Mech. Rock Eng.* **2005**, *38*, 69–76. [[CrossRef](#)]

13. Yilmaz, I. Influence of water content on the strength and deformability of gypsum. *Int. J. Rock Mech. Min. Sci.* **2010**, *47*, 342–347. [[CrossRef](#)]
14. Vishal, V.; Ranjith, P.G.; Singh, T.N. An experimental investigation on behaviour of coal under fluid saturation, using acoustic emission. *J. Nat. Gas Sci. Eng.* **2015**, *22*, 428–436. [[CrossRef](#)]
15. Yu, L.; Yao, Q.; Li, X.; Wang, W.; Han, H.; Zhang, M. Experimental study of failure characteristics and fissure propagation in hydrous siltstone. *Arab. J. Geosci.* **2020**, *13*, 527. [[CrossRef](#)]
16. Roy, D.G.; Singh, T.N.; Kodikara, J.; Das, R. Effect of Water Saturation on the Fracture and Mechanical Properties of Sedimentary Rocks. *Rock Mech. Rock Eng.* **2017**, *50*, 2585–2600. [[CrossRef](#)]
17. Rudajev, V.; Vilhelm, J.; Lokajicek, T. Laboratory studies of acoustic emission prior to uniaxial compressive rock failure. *Int. J. Rock Mech. Min. Sci.* **2000**, *37*, 699–704. [[CrossRef](#)]
18. Backers, T.; Stanchits, S.; Dresen, G. Tensile fracture propagation and acoustic emission activity in sandstone: The effect of loading rate. *Int. J. Rock Mech. Min. Sci.* **2005**, *42*, 1094–1101. [[CrossRef](#)]
19. Cai, M.; Kaiser, P.K.; Morioka, H.; Minami, M.; Maejima, T.; Tasaka, Y.; Kurose, H. FLAC/PFC coupled numerical simulation of AE in large-scale underground excavations. *Int. J. Rock Mech. Min. Sci.* **2007**, *44*, 550–564. [[CrossRef](#)]
20. Ganne, P.; Vervoort, A.; Wevers, M. Quantification of pre-peak brittle damage: Correlation between acoustic emission and observed micro-fracturing. *Int. J. Rock Mech. Min. Sci.* **2007**, *44*, 720–729. [[CrossRef](#)]
21. Ohno, K.; Ohtsu, M. Crack classification in concrete based on acoustic emission. *Constr. Build. Mater.* **2010**, *24*, 2339–2346. [[CrossRef](#)]
22. Sun, X.; Xu, H.; Zheng, L.; He, M.; Gong, W. An experimental investigation on acoustic emission characteristics of sandstone rockburst with different moisture contents. *Sci. China Technol. Sci.* **2016**, *59*, 1549–1558. [[CrossRef](#)]
23. Yang, K.; Yan, Q.X.; Zhang, C.A.; Wu, W.; Wan, F. Study on mechanical properties and damage evolution of carbonaceous shale under triaxial compression with acoustic emission. *Int. J. Damage Mech.* **2021**, *30*, 899–922. [[CrossRef](#)]
24. Chen, L.H.; Chen, W.C.; Chen, Y.C.; Benyamin, L.; Li, A.J. Investigation of Hydraulic Fracture Propagation Using a Post-Peak Control System Coupled with Acoustic Emission. *Rock Mech. Rock Eng.* **2015**, *48*, 1233–1248. [[CrossRef](#)]
25. Chen, L.; Zhao, J.; Zheng, Z. Acoustic Emission Characteristics of Compressive Deformation and Failure of Siltstone under Different Water Contents. *Adv. Mater. Sci. Eng.* **2017**, *2017*, 4035487. [[CrossRef](#)]
26. Carpinteri, A.; Corrado, M.; Lacidogna, G. Heterogeneous materials in compression: Correlations between absorbed, released and acoustic emission energies. *Eng. Fail. Anal.* **2013**, *33*, 236–250. [[CrossRef](#)]
27. Amann, F.; Button, E.A.; Evans, K.F.; Gischi, V.S.; Blumel, M. Experimental Study of the Brittle Behavior of Clay shale in Rapid Unconfined Compression. *Rock Mech. Rock Eng.* **2011**, *44*, 415–430. [[CrossRef](#)]
28. Xiao, F.; He, J.; Liu, Z.; Shen, Z.; Liu, G. Analysis on warning signs of damage of coal samples with different water contents and relevant damage evolution based on acoustic emission and infrared characterization. *Infrared Phys. Technol.* **2019**, *97*, 287–299. [[CrossRef](#)]
29. Rodriguez, P.; Celestino, T.B. Application of acoustic emission monitoring and signal analysis to the qualitative and quantitative characterization of the fracturing process in rocks. *Eng. Fract. Mech.* **2019**, *210*, 54–69. [[CrossRef](#)]
30. Liu, H.L.; Zhu, W.C.; Yu, Y.J.; Xu, T.; Li, R.F.; Liu, X.G. Effect of water imbibition on uniaxial compression strength of sandstone. *Int. J. Rock Mech. Min. Sci.* **2020**, *127*, 104200. [[CrossRef](#)]
31. Huang, S.B.; He, Y.B.; Liu, G.F.; Lu, Z.X.; Xin, Z.K. Effect of water content on the mechanical properties and deformation characteristics of the clay-bearing red sandstone. *Bull. Eng. Geol. Environ.* **2021**, *80*, 1767–1790. [[CrossRef](#)]
32. Huang, Y.M.; Deng, J.H.; Zhu, J. An Experimental Investigation of Moisture-Induced Softening Mechanism of Marble Based on Quantitative Analysis of Acoustic Emission Waveforms. *Appl. Sci.* **2019**, *9*, 446. [[CrossRef](#)]
33. Sagar, R.V.; Prasad, B.K.R. A review of recent developments in parametric based acoustic emission techniques applied to concrete structures. *Nondestruct. Test Eval.* **2012**, *27*, 47–68. [[CrossRef](#)]
34. Meng, Y.Y.; Jing, H.W.; Liu, X.W.; Yin, Q.; Wei, X.C. Experimental and numerical investigation on the effects of bedding plane properties on the mechanical and acoustic emission characteristics of sandy mudstone. *Eng. Fract. Mech.* **2021**, *245*, 107582. [[CrossRef](#)]
35. Wang, H.J.; Liu, D.; Cui, Z.D.; Cheng, C.; Jian, Z. Investigation of the fracture modes of red sandstone using XFEM and acoustic emissions. *Theor. Appl. Fract. Mech.* **2016**, *85*, 283–293. [[CrossRef](#)]